Open birdcage coil for head imaging at 7T

Anton V Nikulin, Alexandre Vignaud, Nikolai Avdievich, Djamel Berrahou, Julien Rosny, Abdelwaheb Ourir

Open birdcage coil for head imaging at 7T

Anton V. Nikulin*[1], Alexandre Vignaud[2], Nikolai I. Avdievich[3], Djamel Berrahou[4], Julien de Rosny[1], and Abdelwaheb Ourir[1]

[1]Institut Langevin, ESPCI Paris, CNRS, PSL University, Paris, France
[2]CEA, DRF, JOLIOT, NeuroSpin, CNRS, Universite Paris-Saclay, Gif-sur-Yvette, France
[3]Max Planck Institute for Biological Cybernetics, Tubingen, Germany
[4]Multiwave Innovation SAS, Marseille, France

September 27, 2022

Abstract

Purpose: To theoretically describe, design and test an open head birdcage coil, called opencage, that facilitates access to the patient under examination. This access improves the patient's comfort, but also may be suitable for many tasks, for example fMRI or motion correction.
Theory and Methods: Using transfer matrix approach, the birdcage-like coil having non-periodical distribution of rungs is constructed with optimized currents in the coil's rungs. Subsequently, the the coil was adjusted in full-wave simulations. Eventually, these results were confirmed on phantom and in-vivo imaging.
Results: Indeed, the high enough computed isolation coefficient between the feeding ports of the coil as well as a birdcage-like B_1^+ pattern showed that the coil was properly optimized. After the numerical optimization, the coil was assembled and fine tuned and matched on the bench. Experimental assessment of the developed coil showed slightly lower B_1^+ homogeneity, competitive transmit efficiency and coverage to the birdcage coil of comparable size.
Conclusion: It was shown that the proposed open birdcage coil can be designed without dramatic drop of performance by means of B_1 field homogeneity and efficiency, SAR.

keywords : ultra-high-field MRI, brain imaging, birdcage coil, open coil, head coil

*Anton V. Nikulin, Institut Langevin, ESPCI Paris, CNRS, PSL University, Paris, 75005, France, a.v.nikulin@live.ru

1 Introduction

Having an open volume RF coil, like the birdcage but with a few removed legs, may be desirable in many clinical and preclinical applications wherein access to the inner volume is needed, for example fMRI when sending optical stimuli with lesser [14], thermal therapy [24] or motion correction [9]. In addition, such a coil makes MRI screening more comfortable, especially, for patients suffering of claustrophobia. There are diversity of known open half-volume RF coils that may be exploited for applications stated above. Among them, for example, phased array coils can successfully resolve the stated issue. In particular, arrays' geometry and currents distribution can be shaped almost at will [3], [25], [7] because the array's elements are well decoupled between each other. Despite all the advantageous of phase arrays, the conventional the birdcage coil still remains common and reliable for transmit regime at UHF MRI such as 7T because of complexity, costliness of the arrays. Contrary to this, in the receive regime use of phased arrays is preferable [27] because of the SNR gain. Nevertheless, as a proof of concept we use the developed open birdcage coil as a transceiver coil for the simplicity.

In the conventional birdcage coil, the rungs, circumscribing an imaged object, are usually densely distributed. Birdcages are typically shielded to prevent interactions with a gradient system of an MRI and to reduce the radiation losses. In addition to volume coils, there is a branch of half-volume coils such as half-birdcage coils [4], U-shaped birdcage coils [15] or quadrature half-volume TEM coils [22] that can also be used for our purposes. However, the B_1 field coverage that we call field of view of the coil (FOV) for the mentioned above coils is still narrower than the FOV of full volume coils like a birdcage coil [13], [12]. The birdcage coil provides suitable B_1 coverage in the brain compared to the half-volume coils [4]. Contrariwise, access to a sample is restricted due to the dense arrangement of the conductive rungs compared to half-volume coils. Thus, another option would be to decrease the number of the rungs to provide wider access between them, but that option leads to a loss of homogeneity and SAR values [19] as shown further. Hence, designing the efficient RF coils that are able to provide such access to the sample without these flaws is an interesting task to be resolved.

For that purpose, we propose an open birdcage head coil wherein a few legs in the top side are removed in order to facilitate access to the inner spacing of the volume coil. We called this RF coil "opencage" coil. The proposed opencage necessitates the realization of an aperiodic structure with a given currents distribution on the rungs. An approach to set the current distribution could have been based on a brute-force electrical engineering approach. This solution was early used to develop elliptical or oval birdcage coils [17], [16], [8]. However, such an approach is not suitable for an arbitrary distribution of the legs. To that end, here we propose to employ an approach wherein the opencage coil is considered as a Transmission Line (TL)-based coil in which we adjust the phase shift per the unit cell and characteristic impedance between different parts of such a TL.

2 Theory and methods

2.1 Calculations of currents and equivalent model of the coil

The development of the opencage coil requires the optimization of the current distribution on each radiating element of the coil (rung or unit cell). In other words, the rungs distributions may arbitrary be changed, but current distribution should retain the same as in the conventional birdcage coil. We propose to achieve this currents modifications in the opencage coil using the formalism of TL with lumped elements (LC). This method has already been used to design the linear polarized opencage coil for preclinical imaging of small animals at 7 Tesla [20]. However, here we address the more complicated challenge of generating the circular polarization (CP) mode improving the efficiency of the coil [10]. Moreover, the enlarged size of the coil leads to certain engineering difficulties because of small values of the used capacitance needed to tune the coil [6].

The aim of this work is to design an opencage coil for UHF head anatomical imaging at 7T operating at the frequency of proton ^{1}H (298 MHz). We set the geometrical parameters to: the inner radius of 130 mm, the length 240 mm, the radius of RF shield is 155 mm, and the leg and ring widths are first equal to 10 mm. These dimensions that are typical for head coils, were used for calculating of the mutual and self-inductances estimated in accordance with [6], [11], [21]. In particular, the mutual inductances of legs were estimated using the rule for two parallel wires [11]. The effect of the shield was taken into account as well [11]. The inductance of rings was also estimated according to the rule for two tilted wires [11]. The desgined coil is composed of eight rungs that are separated by 22.5° in the bottom and only two rungs in the top separated by 90°, wherein opening is provided. The sketches of the coil are shown in Figure 1A,B.

As for the birdcage coil, the opencage coil should maintain 90° phase shift between the two feeding ports to generate the CP mode. That phase shift can be obtained with a 90° hybrid coupler or a combination of Wilkinson power divider connected to the coil ports [19]. However, because of the lack of the periodicity for opencage cells, it is more complicated to obtain that 90° between the two rungs.

However, it is important to note that the desired coil cannot be simply obtained by connecting two types of the cell with the right phase shift together. The birdcage coil can be considered as a transmission line (TL) [5], [19], and the task of connecting different unit cells may be considered as a task of impedance matching between two different TLs. In order to show this, we have to consider the equivalent circuit of a unit cell. This circuit of a typical unit cell composed of two capacitances (C_i), one inductance (L_i) and two end-ring inductances ($L_{r,i}$) is shown in Figure 1C. According to [5], for such a unit cell, 2 by 2 transmission matrix or ABCD matrix can be composed as:

$$T_i = \begin{pmatrix} 1 + Z_i Y_i & -\dfrac{Z_i^2 Y_i + 2Z_i}{2} \\ -2Y_i & 1 + Z_i Y_i \end{pmatrix}$$

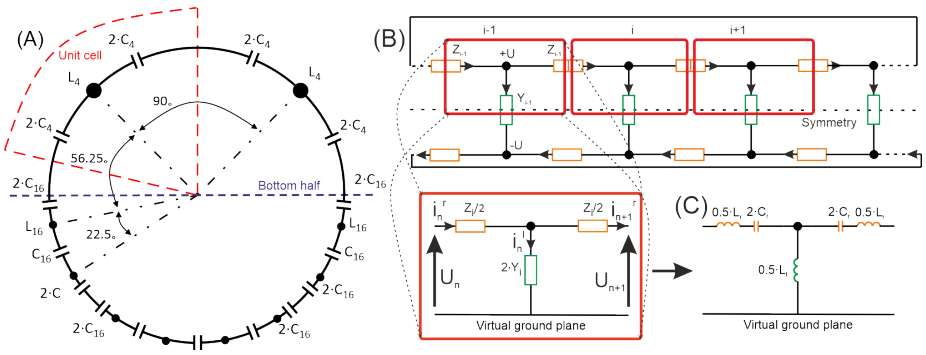

Figure 1: A, Simplified (transverse) representation of an opencage composed of ten rungs. Namely, eight rungs in the bottom and two rungs in the top. B, Equivalent electrical circuit of an opencage. A rung (or unit cell) is represented inside the red line rectangles. Detailed unit cell is shown in the caption (B). C, high-pass unit cell corresponding to the actual unit cell of the opencage coil.

Table 1: Used values of capacitances (C_r) and effective leg inductances (L_l), effective ring inductances (L_r).

Element	22.5° cells (as for 16 rungs)	90° cells (as for 4 rungs)	Modified 90° cells
C_r (pF)	5.15	0.95	1.23
L_i (nH)	173.97	132.6	66.7
L_r (nH)	42.09	165.4	165.4

Where Z_i and Y_i are the impedance and admittance of the unit cell depending on ω, C_i, $L_{r,i}$ and ω, L_i respectively.

From this matrix the Bloch impedance ($Z_{i,b}$) and the relative phase shift ($\delta\varphi_i$) can be evaluated through eigenvalues and eigenvector analysis [19], [5]:

$$\delta\varphi_i = \cos^{-1}\left(1 + Z_i Y_i\right)$$
$$Z_b^i = \frac{1}{2}\sqrt{Z_i^2 + \frac{2Z_i}{Y_i}}$$

From them the leg inductances and ring capacitance can be deduced directly as:

$$L_l = \frac{4{Z_b}^2\,(1-\cos\delta\varphi) - 2\,L_r\,Z_b\,|\sin\delta\varphi|\,\omega}{2Z_b\,|\sin\delta\varphi|\,(1-\cos\delta\varphi)\,\omega - L_r\,\sin^2\delta\varphi\,w^2}$$
$$C = \frac{L_r\,(\cos\delta\varphi+1)\,\omega - 2\,Z_b\,|\sin\delta\varphi|}{{L_r}^2\,(\cos\delta\varphi+1)\,\omega^3 + {Z_b}^2\,(4\cos\delta\varphi-4)\,\omega}$$

First of all, we consider the unit cell with the relative phase shift of 22.5° per rung (as for sixteen rungs birdcage coil). For that geometry, the effective leg and ring inductances were evaluated. The result is shown in Tab. 1).

The same procedure was performed for the 90° cells (as for the four leg birdcage coil). Here we compute the inductances and capacitances of the 90°

cell by considering only the 90° phase shift and retaining the same width for the legs and rings as the one of the 22.5° cells. Taking into account both the 90° phase shift and the Block impedance to be the same as the ones of the 22.5° cells, the width of legs should be modified for the 22.5° and/or for the 90° cells. For that purpose, constrain optimization based on gradient descent method was used to evaluate effective leg inductance (L_i) and capacitance C_i. In that optimization, the Bloch impedance and relative phase shift was set to 62.45 Ohm and 90° respectively. Here, the effective ring inductance $L_{r,i}$ was set constant to 165.4 nH.

The corresponding dispersion curves are shown in Figure 2A. As expected for the three kinds of unit cells (22.5° and the 90° optimized and non-optimized), the phase shifts at 298 MHz reach the expected values. The Bloch impedances were calculated over the same frequency range for the three-unit cells. As it can be seen from Figure 2C, the impedance of the unmodified 90° unit cell is approximately twice higher than that one of the 22.5° unit cell. These two parameters were properly adjusted in order to match each other at the desired frequency. The dispersion and impedance diagrams of this optimized 90° unit cell is presented in Figure 2A,E. Thus, to achieve the desired value of leg inductance, the width of a leg should be increased from 10 mm to 39.5 mm.

2.2 Circuit simulations

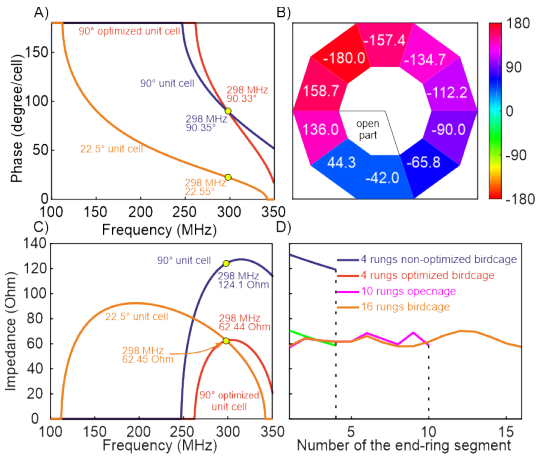

Figure 2: A, Band diagram of three different unit cells. B, current distribution in end-ring segment. C, Bloch impedance for the three different unit cells. D, Impedance in end-ring nods for several birdcage composed of different unit cells.

The additional electrical simulation using the circuit simulator of CST Microwave Suite was performed in order to validate these estimated theoretical values of impedances and phases. Here, the three different birdcages and one opencage were studied: the birdcage with sixteen 22.5° distant cells; the bird-

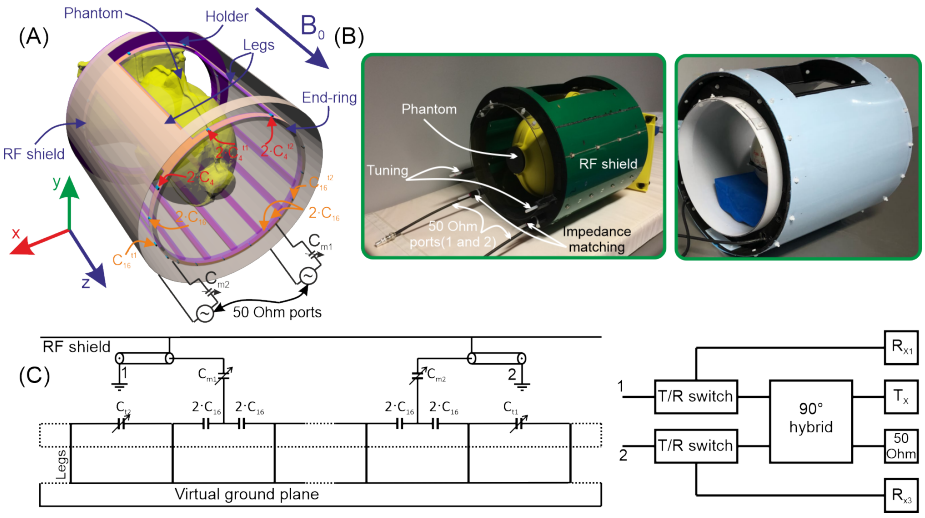

Figure 3: A, Geometry of the loaded opencage coil driven in quadrature. B, Photograph of the opencage coil C, Sketch of the tuning, matching and interfacing circuits.

cage with four 90° distant cells without the impedance optimization; birdcage with four 90° distant cells after the phase and impedance optimization; the optimized opencage. Here, the opencage was modeled as a ten-unit cells (rungs) circuit. The results of that simulation are presented in (Figure 2B,D). First, it can be seen from Figure 2B that the computed phases along the whole transmission line composed of opencage unit cells are consistent with the expected ones. In addition, the Bloch impedance has been assessed by plotting the ratio between voltage and current at the nods.

Eventually, it can be seen in Figure 2D that the impedances are comparable to the expected ones (Figure 2C). Moreover, the computed phases Figure 2B are in the good agreement with the predicted ones (Figure 2A). Therefore, this result fully justifies the metamaterial approach used to retain simultaneously the proper phase shift and the same Bloch impedance as the one of the 22.5° cell. As a result, the coil can be now designed more precisely and investigated in full-wave simulations.

2.3 Design of the opencage coil

The design of the opencage is illustrated in Figure 3A. As it was mentioned in the previous section, the opencage coil has the following geometrical parameters: radius of 130 mm, length of 240 mm, and radius of the RF shield of 155 mm. The coil is shielded by copper list with a gap of 139 mm width in front of the opening (90° rungs). This gap was obviously made in the top part of the coil. The geometrical parameters of the coil were chosen in order to tight fit a head.

The width of end-rings and bottom legs equal 10 mm, while the width of the modified legs in the top is initially set to 39.5 mm. However, we further modified this width to 55 mm in order to optimize the isolation (S_{12}) between the feeding ports in full-wave simulations.

The coil is driven in quadrature by two 50 Ohm ports that are 90° distant at the bottom part (see Figure 3A). The ports are connected between the doubled capacitances in the end-ring segments and the shield, as it is shown in Figure 3A. In this case, the opencage coil is excited thought capacitive coupling.

2.4 Full-wave numerical simulations

Initially, the design was numerically tested and optimized using commercial electromagnetic software CST Studio Suite 2019 (CST, Darmstadt, Germany). In the conducted simulations, the coil was firstly loaded with a homogeneous dielectric sphere phantom of the diameter 165 mm (not shown in Figure 3)A. Its relative permittivity (ε_r) and conductivity (σ) were equal to 75 and 1 S/m respectively. These simulations were done in FEM-based Frequency Domain Solver with approximately 1 million mesh cells.

It appeared that with the values of the capacitors different from the analytical model, the resonance frequency of the simulated opencage is 15% lower than the expected one. As a result, in order to tune the coil to the frequency of 298 MHz, the capacitors were slightly scaled compared to the analytical values. Thus, $2C_4$ becomes 2 pF instead of 2.46 pF and $2C_{16}$ became 8.3 pF instead of 10.3 pF. This 20% of difference between analytically predicted and simulated results may be explained by several factors. First, the geometry of the shield is complex because of the gap at the top. Second, the high index dielectric phantom modifies the mutual inductances. Finally, there is the influence of the two feeding 50 Ohm ports as well as ESR and ESL effects of the used capacitors. Moreover, in order to reduce the number of capacitors, when it is possible, two capacitors in series were replaced by a single capacitor. According to Figure 3, twofold capacities are only retained on the rungs wherein: the feeding ports are connected, the two types of cells are connected, cells are on top part. For this last, this is because the total capacitance of the two $\approx$ 2pF-capacities would have been $\approx$ 1 pF which is below self-parasitic capacity of the coil containing 90° rungs [19].

In order to maximize the isolation level between the feeding port and to maximize the capacitance C_4 needed to tune the coil to the desired frequency, we enlarged the width of the top legs to 55 mm instead of 39.5 mm. Eventually, using the the setup with the adjusted parameters we simulated the B_1^+ at the frequency of interest and further compared it to the experimentally acquired data using the same size phantom.

Eventually, to confirm the necessity of the opening provided by the opencage compared to the birdcage coil with only 4 rungs, and to compare the performance pf the opencage with the common birdcages containing 4 and 16 rungs, we conducted electrodynamics simulations of these three coils. The simulated coils had same sizes in exception of the width of the legs that was different in

these coils, namely 20 mm for the birdcage with 4 rungs, 10 mm for 16 rungs; 10 and 55 mm for the opencage coil. We assessed their performance via the RF safety (SAR) assessment and B_1^+ field computation. To that purpose, we performed an additional computation using CST Microwave suite 2019 in the Time Domain Solver with approximately 8-10 millions of mesh cells. We used multi tissue Ella voxel model cropped at the shoulder level [18], [23]. The model has an isotropic voxel of 2 mm^3 and materials tissue parameters adapted for 297 MHz. In all simulations series the coils were tuned and impedance matched using electrical simulator extension (CST Schematic). In the conducted simulations we evaluated the transmit efficiency (¡B_1^+¿/$\sqrt{P}$) and local maximal SAR_{10g} (averaged for 10 g of tissue) at the frequency of 297.2 MHz. The obtained maps were normalized for the 1W of the stimulated power in order to take into account the influence of the matching level. The B_1^+ homogeneity was also assessed for the considering setups using standard deviation D/ $< B_1^+ >$. At last, we evaluated the radiated power (P_r) for each coil in order to study the effect of opening.

2.5 Prototype assembling

After optimizing parameters of the opencage coil in full-wave simulations and finally tuning the coil to the desired frequency of 297.2 MHz, we proceeded to realizing the desired coil. The photographs of the realized coil iis presented in Figure 3B. The frame of the coil was 3d printed using polylactic acid (PLA). The electrical tracks were made of 35 μm thick copper foil tape. Then, all the components were soldered. The RF shield was chemically etched on FR4 substrate with 5 narrow gaps made along Z axis in the metal layer in order to prevent eddy currents. For that purpose, four nonmagnetic capacitors of 1 nF were soldered between these gaps as proposed in [1].

In the prototype, we used the same values of the capacitors as the ones of the simulation. The tuning and matching circuits were implemented as shown in Figure 3A,C. Two trim capacitors (1-13 pF) connected in series to the feeding lines were employed for impedance matching. In order to tune the resonant frequency, the same kind of variable capacitors were placed instead of the two fixed ones as shown in Figure 3C.

To connect the coil to our Siemens 7T MRI scanner (Erlangen, Germany), the interfacing devices shown in Figure 3C was used. In this interface, each single port of the coil is connected to 90° hybrid coupler in order to have circular polarization in the transmit regime. In receive regime, each port of the coil is connected to its own T/R switch containing low noise preamplifiers, which are finally connected to the receive channels 1 and 3 of the scanner.

2.6 Experimental evaluation

At first, the assembled opencage coil was assessed on the bench with VNA (Anritsu MS46122b) via S-parameters measurements. The coil loaded by the sphere phantom (agar 3%m, NaCl 0.5%m, $NiCl_2$ 0.03%m) was tuned and matched slightly below the exact Larmor frequency of 297.3 MHz, namely at 296.7 MHz

because of the effect of the MRI bore that slightly detunes the coil to the higher frequency.

After fine tuning the coil on the bench, the coil loaded by sphere phantom was installed and connected to our MRI scanner using the Tx/Rx interface described above. Then, the XFL sequence was employed for FA mapping [2], [26] that was latter converted to B_1 maps. The parameters of the used sequence were the following: TR/TE = 20000/3.06 ms, pixel in plane spacing of 4 mm and slice thickness of 8 mm, FOV of 256 mm by 256 mm by 168 mm, FA of 7°, and SAT of 60°. The same sequence was also performed with a commercial non-shielded birdcage coil from Invivo manufacturer. This birdcage has 16 rungs. It also has a 3.3% smaller inner volume (radius of 140 mm and length of 200 mm) compared to the built opencage coil. For both coils we adjusted the reference voltages via the same $^{+}_{1}$ mapping sequence allowing to obtain the reference voltage maps that show the voltage needed to obtain 500 μs rectangular 90° pulse (FA) in the center of the phantom. The measured B_1^+ maps were then acquired with 212 V as the reference voltage for the commercial coil and 174 V for the opencage coil. Based on the obtained maps we evaluated transmit efficiency ($< B_1 > /V_{ref}$) and homogeneity of B_1 via $D/ < B_1^+ >$. For these evaluation we used the data from whole phantom.

At last, in-vivo images and B_1^+ maps in three planes were acquired for the birdcage and for the opencage coil using the in-vivo acquisition protocol followed restricted SAR protocol used locally to test in-house built coils [26]. In addition, obtained B_1^+ maps were smoothed with the median filter. The measured images were acquired with 255 V as reference voltage for the birdcage coil and with 203 V as reference voltage for the opencage coil. After all, the obtained images were filtered using the amplitude of FA map as well as smoothing with median filter. For these obtained data we also estimated transmit efficiency ($< B_1 > /V_{ref}$) and homogeneity via $D/ < B_1^+ >$. For assessing the overall transmit efficiency and homogeneity we used the average value over the three orthogonal slices.

3 Results

3.1 Numerical optimization of the coil

Before assembling the prototype, we optimized the width of the top leg in the opencage coil loaded by the sphere phantom. To that end we plotted the ($|S_{12}|$) isolation between the feeding ports depending on the width (Figure 4). The lowest $|S_{12}|$ coefficient appears for the width of approximately 55 mm. Moreover, we observe that increase in width moves the k=1 mode to the higher frequency, due to decrease in leg inductance. Thus, this increase in leg width was used to shift the k=1 mode toward the desired Larmor frequency of 297.2 MHz without reducing the capacitance.

After optimizing this width, we computed the B_1^+ maps for the birdcage of 4 rungs (Figure 5A), 16 rungs (Figure 5B) and for the opencage coil (Figure 5C). The top row in Figure 5 shows the simulated setup of three types of coils,

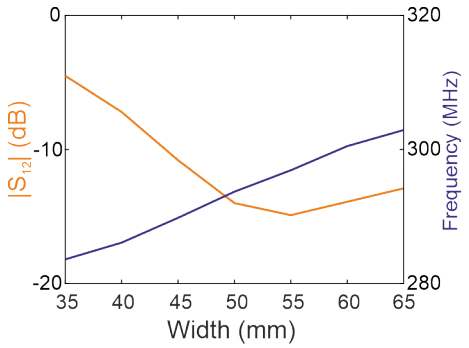

Figure 4: Isolation (left axis) and resonant frequency (right axis) depending on the top legs width.

Table 2: Numerical comparison of different volume coils for 1W of stimulated power.

Coil	¡B_1^+¿/$\sqrt{P}$ (μT/$\sqrt{W}$)	SAR_{10g} (W/kg)	D/ $< B_1^+ >$	P_r (W)
4 rungs birdcage	0.358	0.599	0.263	0.176
16 rungs birdcage	0.370	0.458	0.245	0.166
Opencage	0.365	0.519	0.245	0.216

the second row presents of B_1^+ distribution in the central sagittal plane, at last, the field in the central transverse plane is presented in the bottom row. First of all, these simulated results shows the rightness of optimization strategy because the field distribution of the opencage coil corresponds to the conventional CP mode of the birdcage coil having the maximum of field in the center and decaying toward the periphery. The opencage shows also acceptable symmetry with respect to its vertical axis. The quantitative assessment of efficiency of each simulated coil are arranged in Table 2.

At first, as it can be seen in Table 2, the mean transmit efficiency in the ROI (¡B_1^+¿/$\sqrt{P}$) is not strongly affected by the number of legs. For the developed opencage coil this value is in between the birdcage of 16 rungs and birdcage with only 4 rungs. In addition, one can conclude that opening made in the top of the coil slightly increased the radiated power, however, the transmit efficiency is not dramatically affected by this increase in P_r. In terms of homogeneity, which was assessed as the standard deviation (SD) over ¡B_1^+¿, the birdcage of 4 rungs shows the worst results. However, this is not an explore because it is well known that homogeneity of B_1^+ depends on the number of rungs [19]. It was expected for the opencage coil to be in between the 4 rungs and 16 rungs birdcages, whereas, the opencage shows unexpectedly high values of D/ $< B_1^+ >$ for the chosen ROI (white rectangle in Figure 5). However, it can be explained by the wider legs in the top of the coil, that compensates the drops of the field attributed to birdcage with lower amount of the rungs.

However, before going toward the experimental realization, SAR assessment

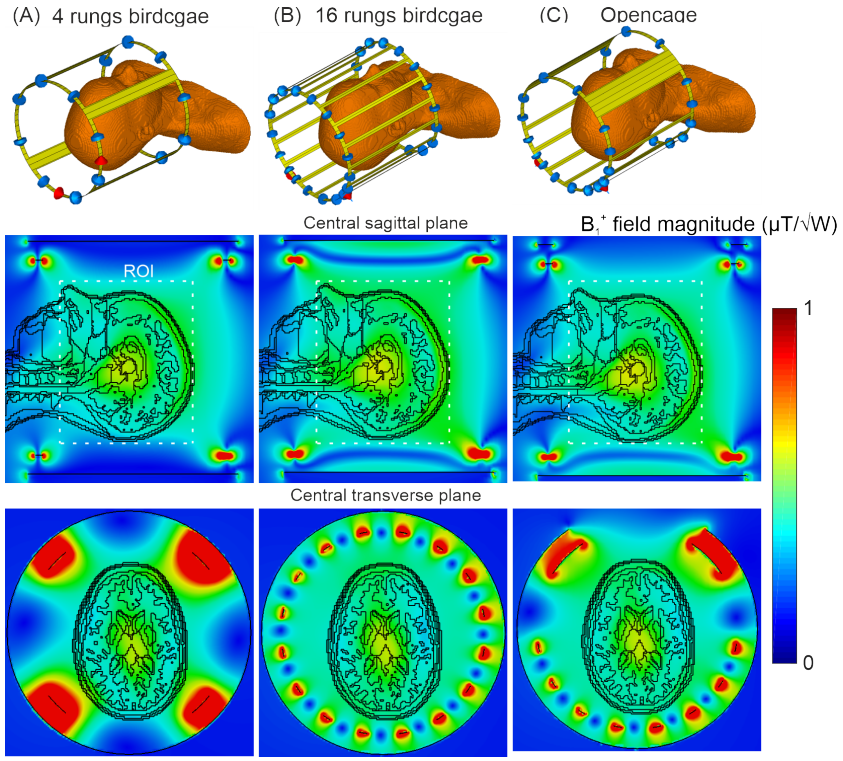

Figure 5: A, B_1 maps obtained in numerical computation obtained for the birdcage coil of 4 rungs. B, simulated B_1 maps for the birdcage coil of 16 rungs. C, simulated B_1 maps for the opencage coil. The RF shield is hidden in all the setups. The top row shows the simulated setup. The maps obtained in central sagittal plane are depicted in the middle. The bottom line shows the fields in the central transverse plane. The ROI is limited by white dashed rectangle in sagittal slice. The full size of the ROI is 150 mm along x axis, 205 mm along y axis, 180 mm along z.

should be provided as a part of ethical committee assessment before acquiring in-vivo data. The quantitative analysis of SAR is summarized in Table 2. The maximum SAR_{10g} maps are plotted in Figure 6, in which the top row shows central sagittal plane, whereas lower row presents transverse plane of the maximum value of SAR_{10g} at the position of z=-55.7 mm. The results for the birdcage of 4 rungs are presented in Figure 6A, for 16 rungs in Figure 6B, and for the opencage in Figure 6C. One observes the two SAR spots, the first one is in the vertex. In this area the SAR slightly increases with increase the number of the legs, as it can be observed in the top raw of Figure 6. However, the peak values are observed at the nose. In this case the SAR decreases with increase the number of the legs.

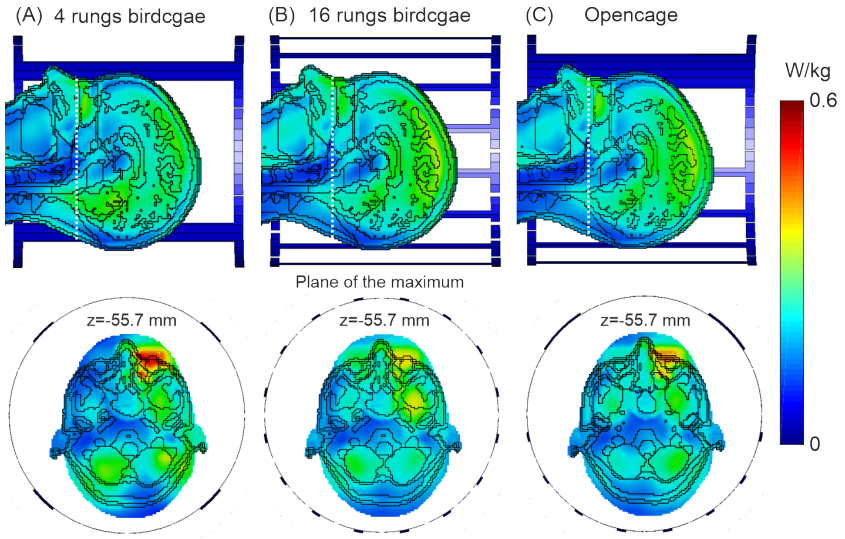

Figure 6: A, Numerically estimated local SAR for 10 g of tissues for the 4 rungs birdcage coil. B, for the 16 rungs birdcage coil. C, for the opencage coil. All maps were normalized for 1 W of stimulated power. Top row shows the maps in the central sagittal plane. Low row presents the maps the transverse plane of the maximum. The position of the maximum is shown by white dashed line with coordinate z of -55.7 mm.

3.2 Imaging with the opencage coil

After studying the opencage coil using electrodynamics full-wave simulations, we first performed the study on the bench. At first the coil was tuned to the frequency of 297.2 MHz and matched in the presence of the sphere agar phantom at the level of -26 dB, while isolation level between the ports was -12.5 dB.

Subsequently, we measured B_1^+ maps in the sphere phantom. These maps are shown in Figure 7. Figure 7A shows the simulated and measured maps using the opencage coil, Figure 7B shows the measured map of the commercial birdcage coil. As first, we evaluated the transmit efficiency of the obtained images. Being normalized to reference voltage, the transmit efficiency ($< B_1 > /V_{ref}$) of the birdcage equals 0.017 μT/V in the center of the maps, while for the opencage it equals 0.026 μT/V, which is 34.6% greater.

According to the acquired data, we calculated $D/ < B_1^+ >$ in the both data sets. The birdcage coil demonstrated slightly better homogeneity of B_1^+ in the entire phantom. The estimated $D/ < B_1^+ >$ for the entire phantom equals 0.214 for the birdcage coil and 0.223 (-4%) for the opencage coil.

At last, three in-vivo images and B_1^+ maps were acquired for the birdcage (Figure 8A, B) and for the opencage coils (Figure 8C, D). As in the case of the sphere phantom, in in-vivo the opencage shows superior performance then that on of the birdcage coil. Being normalized to reference voltage, the transmit

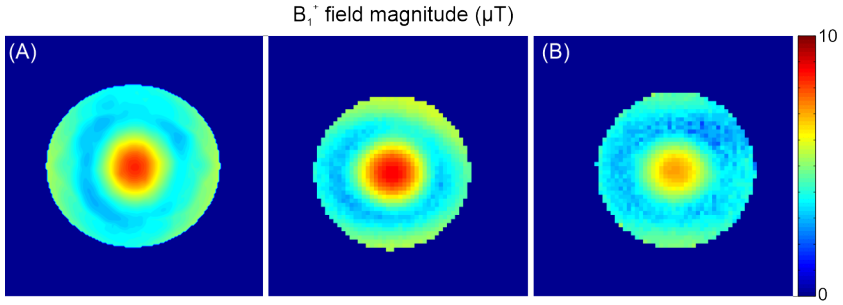

Figure 7: A, simulated and measured B_1^+ field in the central sagittal slice for the opencage coil loaded by the sphere phantom. B, measured B_1^+ map for the commercial birdcage coil.

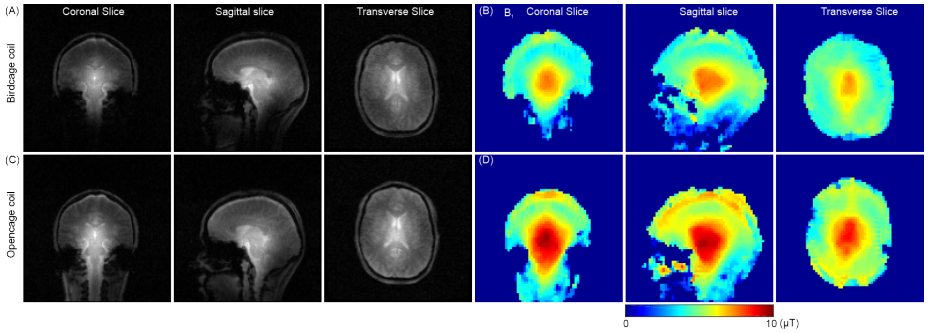

Figure 8: A, In-vivo images (a.u.) of the brain obtained in the three central slices for the birdcage coil. B, B_1^+ maps (μT) obtained with birdcage coil in three slices. C, In-vivo images from three slices for the opencage coil. D, B_1^+ maps obtained with opencage coil.

efficiency ($< B_1 > /V_{ref}$) of the birdcage equals 0.018 μT/V, while for the opencage it equals 0.028 μT/V, which is 35.7% greater. This dramatic enhance in transmit efficiency can be explained by the fact that used birdcage coil is not shielded, and it was not well tuned inside the new gradient system. This higher transmit efficiency ($< B_1 > /V_{ref}$), reciprocally improves the obtained brain images (Figure 8C). Moreover, we estimated the $D/ < B_1^+ >$ for both coils that is equal to 0.284 for the birdcage coil and to 0.306 (-6.3%) for the opencage coil. These images are shown in Fig. 8A for the birdcage coil, and in Figure 8C for the opencage coil. Eventually, we can conclude that opencage coil is also slightly better in terms of B_1 coverage compared to the birdcage coil.

4 Discussion

We have designed an open birdcage coil containing different kind of the unit cells (Figure 1 and Figure 3). This opencage not only improves the comfort of patients under examination, but also may be required for many tasks, such as fMRI wherein sending optical stimuli with lesser is needed [14], thermal therapy [24], motion correction [9], and other wherein the opening may be required. Our aim of this work was to show the competitive to a conventional birdcage coil performance in terms of B_1 homogeneity and transmit efficiency. The opencage can be constructed using a novel approach of optimization of currents using transmission matrix approach. At first, we optimized the impedance and phases of different birdcages containing different number of the rungs (Figure 2A, C). These rungs can be represented by different leg inductance values (leg width), that finally tunes the capacitance needed to tune the k=1 mode at the right frequency [6]. After optimizing this values analytically, we used commercial RF circuit simulator (CST Studio) in order to confirm the obtained values of the impedance and phases (Figure 2B, D).

Then, the coil was tuned to the right frequency and the isolation between the port was adjusted with the parameters sweep over the optimal legs that was found via full-wave simulations presented in Figure 4. That configuration was then fully tested in electrodynamics simulations (Figure 5) in the presence of the Ella voxel model [18], [23]. This configuration was also compared to the birdcage coils containing 4 and 16 rungs. The conducted simulations showed that the developed opencage coil and birdcage coils showed 7% better homogeneity of B_1 assessed via SD shown in Table 2. The average transmit efficiency was not strongly affected by the number of the unit cell. Before manufacturing, we provided the SAR analysis as well. As it is denoted in Table 2, the birdcage of 16 rungs shows the best RF safety, and moreover, this RF safety depends on the number of the legs. Thus, the opencage demonstrated 13.4% lower local SAR_{10g} for 1W of stimulated power, whereas it was 11.8% higher compared to the birdcage coil. Thereby, one can conclude that the opencage provide a compromise by the means of RF safety between the birdcage of 4 and 16 rungs. RF safety is important and critical parameter of the Tx coils involved for in-vivo applications, consequently, assessing the SAR (Figure 6) we confirmed the importance of the conducted optimization and clearly see the benefits compared to the birdcage coil of only 4 rungs. Therefore, the interest of the concept of opencage coil is clearly seen here. Opening in the coil cannot be simply provided by the decreasing the number of legs because of the SAR, which in the case of our opencage coil is a trade-off between birdcage of 4 rungs and the birdcage coil of 16 rungs. However, it is not a surprise, and it was expected because in the birdcage-like coil the electrical field is confined around the legs. While in the birdcage with 16 rungs, the electrical field is smoother distributed between all the legs compared to the birdcage with only 4 rungs. In addition, smaller capacitances in the birdcage of 4 legs also increase the electric field.

By analysing the experimental data obtained with spherical phantom (Figure 7), one can conclude that the opencage shows 4% worse homogeneity for

the whole sphere phantom, assessed via $D/ < B_1^+ >$ then that one of the birdcage coil, and 6.3% homogeneity drop for the in-vivo acquisition (Figure 8B,D). While simulations shows comparable homogeneity via SD in voxel head phantom (Table 2). However, these two considered configuration cannot be compared directly because the coils have different size, whereas the simulated coils have the same size. Therefore, it is more interesting to compare these values of SD obtained in-vivo. The opencage is more efficient in transmit efficiency even though it has 3.3% bigger inner spacing. This dramatic enhance in transmit efficiency (34.6%) for the sphere phantom, and 35.7% greater for the in-vivo, can be explained by the fact that used commercial coil is not shielded, and it was not properly tuned after installation of the new gradient system.

5 Conclusion

In this work, we proposed a new type of RF quadrature coil, named opencage, that facilitates access to the region under study. That opening may be useful for improving patients' comfort and for some task like motion correction in MRI, and fMRI. This coil was optimized for head imaging at 7T. The proposed RF coil is based on Bloch impedance matching and the phase adjustment. The main parameters of the opencage coil were determined analytically, tested numerically, and confirmed experimentally on the bench and in MRI. Eventually, the opencage coil demonstrated a slightly lower homogeneity ($D/ < B_1^+ >$) of 6.3% and competitive transmit efficiency ($< B_1 > /V_{ref}$).

acknowledgements

This project has received funding from the European Union's Horizon 2020 research and innovation program under Grant Agreement No. 736937. This work is supported by LABEX WIFI (Laboratory of Excellence within the French Program "Investments for the Future") under references ANR-10-LABX-24 and ANR-10- IDEX-0001-02 PSL. This work has been supported by the Leducq Foundation (large equipment ERPT program, NEUROVASC7T project).

References

[1] Marcello Alecci and Peter Jezzard. Characterization and reduction of gradient-induced eddy currents in the RF shield of a TEM resonator. *Magnetic Resonance in Medicine*, 48(2):404–407, aug 2002.

[2] Alexis Amadon, Martijn Anton Cloos, Nicolas Boulant, Marie-France Hang, Christopher John Wiggins, and Hans-Peter Fautz. Validation of a very fast B1-mapping sequence for parallel transmission on a human brain at 7T. *MRM*, 60(9):84, 2008.

[3] Nikolai I Avdievich. Transceiver-Phased Arrays for Human Brain Studies at 7 T. *Applied Magnetic Resonance*, 41(2-4):483–506, dec 2011.

[4] D Ballon, M C Graham, S Miodownik, and J A Koutcher. A 64 MHz half-birdcage resonator for clinical imaging. *Journal of Magnetic Resonance (1969)*, 90(1):131–140, oct 1990.

[5] Christophe Caloz and Tatsuo. Itoh. *Electromagnetic metamaterials : transmission line theory and microwave applications : the engineering approach*. John Wiley & Sons, 2006.

[6] Chih-Liang Chin, Christopher M. Collins, Shizhe Li, Bernard J. Dardzinski, and Michael B. Smith. BirdcageBuilder: Design of specified-geometry birdcage coils with desired current pattern and resonant frequency. *Concepts in Magnetic Resonance*, 15(2):156–163, jun 2002.

[7] Jérémie Clément, Rolf Gruetter, and Özlem Ipek. A combined 32-channel receive-loops/8-channel transmit-dipoles coil array for whole-brain MR imaging at 7T. *Magnetic Resonance in Medicine*, page mrm.27808, may 2019.

[8] Nicola De Zanche, Atiyah Yahya, Fred. E. Vermeulen, and Peter S. Allen. Analytical approach to noncircular section birdcage coil design: Verification with a Cassinian oval coil. *Magnetic Resonance in Medicine*, 53(1):201–211, jan 2005.

[9] Robert Frost, Paul Wighton, F. Işık Karahanoğlu, Richard L. Robertson, P. Ellen Grant, Bruce Fischl, M. Dylan Tisdall, and André van der Kouwe. Markerless high-frequency prospective motion correction for neuroanatomical MRI. *Magnetic Resonance in Medicine*, 82(1):126–144, jul 2019.

[10] G. H. Glover, C. E. Hayes, N. J. Pelc, W. A. Edelstein, O. M. Mueller, H. R. Hart, C. J. Hardy, M. O'Donnell, and W. D. Barber. Comparison of linear and circular polarization for magnetic resonance imaging. *Journal of Magnetic Resonance (1969)*, 64(2):255–270, sep 1985.

[11] Frederick W. Grover. *Inductance Calculations: Working Formulas and Tables*. Dover publications, 1971.

[12] Cecil E. Hayes. The development of the birdcage resonator: a historical perspective. *NMR in Biomedicine*, 22(9):908–918, nov 2009.

[13] Cecil E Hayes, William A Edelstein, John F Schenck, Otward M Mueller, and Matthew Eash. An efficient, highly homogeneous radiofrequency coil for whole-body NMR imaging at 1.5 T. *Journal of Magnetic Resonance (1969)*, 63(3):622–628, 1985.

[14] Ruey Song Huang and Martin I. Sereno. Visual stimulus presentation using fiber optics in the MRI scanner. *Journal of Neuroscience Methods*, 169(1):76–83, mar 2008.

[15] Alex M J Hudson, Walter Köckenberger, and Richard W Bowtell. Open access birdcage coils for microscopic imaging of plants at 11.7T. *Magma: Magnetic Resonance Materials in Physics, Biology, and Medicine*, 10(2):69–74, jun 2000.

[16] Mark C. Leifer. Theory of the quadrature elliptic birdcage coil. *Magnetic Resonance in Medicine*, 38(5):726–732, nov 1997.

[17] Shizhe Li, Christopher M. Collins, Bernard J. Dardzinski, Chih-Liang Chin, and Michael B. Smith. A method to create an optimum current distribution and homogeneous B1 field for elliptical birdcage coils. *Magnetic Resonance in Medicine*, 37(4):600–608, apr 1997.

[18] Xin Li and Joseph V. Rispoli. Toward 7T breast MRI clinical study: safety assessment using simulation of heterogeneous breast models in RF exposure. *Magnetic Resonance in Medicine*, 81(2):1307–1321, feb 2019.

[19] Joël Mispelter, Mihaela Lupu, and André Briguet. *NMR Probeheads for Biophysical and Biomedical Experiments*. IMPERIAL COLLEGE PRESS, jul 2015.

[20] A Nikulin, J De Rosny, K Haliot, B Larrat, and A Ourir. Opencage radio frequency coil for magnetic resonance imaging. *Applied Physics Letters*, 114(5), feb 2019.

[21] Romeo Pascone, Thomas Vullo, John Farrelly, and Patrick T. Cahill. Explicit treatment of mutual inductance in eight-column birdcage resonators. *Magnetic Resonance Imaging*, 10(3):401–410, 1992.

[22] A S Peshkovsky, R P Kennan, M E Fabry, and Nikolai I Avdievich. Open half-volume quadrature transverse electromagnetic coil for high-field magnetic resonance imaging. *Magnetic Resonance in Medicine*, 53(4):937–943, apr 2005.

[23] Joseph V Rispoli, Steven M Wright, Craig R Malloy, and Mary P McDougall. Automated modification and fusion of voxel models to construct body phantoms with heterogeneous breast tissue: Application to MRI simulations. *Journal of Biomedical Graphics and Computing*, 7(1):1, feb 2017.

[24] Usama Salem, Vinodh A Kumar, John E Madewell, Donald F Schomer, Dhiego Chaves de Almeida Bastos, Pascal O Zinn, Jeffrey S Weinberg, Ganesh Rao, Sujit S Prabhu, and Rivka R Colen. Neurosurgical applications of MRI guided laser interstitial thermal therapy (LITT). *Cancer Imaging*, 19(1):65, dec 2019.

[25] Shubharthi Sengupta, Alard Roebroeck, Valentin G. Kemper, Benedikt A. Poser, Jan Zimmermann, Rainer Goebel, and Gregor Adriany. A Specialized Multi-Transmit Head Coil for High Resolution fMRI of the Human Visual Cortex at 7T. *PLOS ONE*, 11(12):e0165418, dec 2016.

[26] Alexandre Vignaud, Franck Mauconduit, Vincent Gras, Nicolas Boulant, Olivier Girard, Alexander Raaijmakers, Frank Kober, Denis Le Bihan, and Redha Abdeddaim. Fast and unconditionally safe in vivo MR head protocol for home-made coil prototype assessment at 7T. *Journal of Physics: Conference Series*, 1092:012159, 2018.

[27] G C Wiggins, C J Wiggins, A Potthast, V Alagappan, O Kraff, A Reykowski, and L L Wald. A 32 Channel Receive-only Head Coil And Detunable Transmit Birdcage Coil For 7 Tesla Brain Imaging. Technical report, 2006.